Chemical Engineering Science 129 (2015) 249–259

Contents lists available at ScienceDirect

Chemical Engineering Science

journal homepage: www.elsevier.com/locate/ces

# Mechanistic evaluation of hematin action as a horseradish peroxidase biomimetic on the 4-aminoantipyrine/phenol oxidation reaction

A. Córdoba [a,1], N. Alasino [a,1], M. Asteasuain [b,2], I. Magario [a,*,1], M.L. Ferreira [b,2]

[a] Investigación y Desarrollo en Tecnología Química (IDTQ), Grupo Vinculado PLAPIQUI—CONICET, Facultad de Ciencias Exactas, Físicas y Naturales, Universidad Nacional de Córdoba, Córdoba, Argentina

[b] Planta Piloto de Ingeniería Química (PLAPIQUI), PLAPIQUI-UNS-CONICET, Universidad Nacional del Sur, Bahía Blanca, Argentina

## HIGHLIGHTS

- Hematin catalytic action towards phenol was modelled and validated.
- Horseradish peroxidase catalytic intermediaries are also operative for hematin.
- Kinetic modelling allowed identifying relevant catalytic and deactivation routes.
- Existence of peroxide radicals during phenol oxidation is postulated for hematin.
- Hematin emerges as less-expensive alternative for the Trinder's reaction.

## GRAPHICAL ABSTRACT

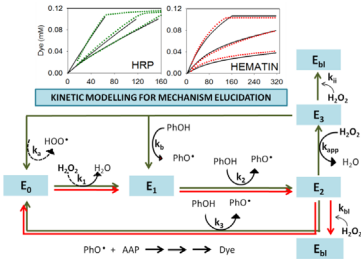


## ARTICLE INFO

*Article history:*
Received 21 November 2014
Received in revised form
6 February 2015
Accepted 21 February 2015
Available online 6 March 2015

*Keywords:*
Biomimetics
Peroxidase
Bioprocess monitoring
Dynamic simulation
4-Aminoantipyrine
Kinetic parameters

## ABSTRACT

Hematin, a mimetic structure of heme peroxidases, was successfully applied for $H_2O_2$-mediated condensation reaction between phenol and 4-aminoantipyrine. The catalytic action was evaluated in comparison to horseradish peroxidase (HRP) by kinetic modelling and parametrization procedure. Expected side reactions were checked and discarded as model-relevant routes. The existence of the oxoperferryl-π-cation radical and oxoperferryl species of hematin, as analogues of Compounds I and II of HRP, can be postulated because simulated product formation fitted experimental data. However, in light of the optimized rate constants encountered, hematin was less active to peroxide activation and less specific to the coordination of phenol vs. $H_2O_2$ than HRP. The model indicated that hematin bleaching from key intermediate oxoperferryl was induced rather than regenerated via Compound III formation. In contrast to the enzyme, the faster oxygen evolvement and the lack of precipitating polyphenol production observed with hematin after 4-aminoantipyrine depletion were interpreted as accumulation of oxidising HOO• radicals through the peroxide decomposition pathway. This study may be of interest for interpreting the catalytic performance of hematin. Moreover, the replacement of the enzyme by the less-expensive and non-polyphenol-forming hematin for this versatile colorimetric assay may provide convenient results, especially in flow-injection modes and analytical columns applications.



* Corresponding author. Tel.: +54 351 5353800(29783).
*E-mail addresses:* agostinacordoba@gmail.com (A. Córdoba), nalasino@santafe-conicet.gov.ar (N. Alasino), masteasuain@plapiqui.edu.ar (M. Asteasuain), imagario@efn.uncor.edu (I. Magario), mlferreira@plapiqui.edu.ar (M.L. Ferreira).
[1] Address: Av. Velez Sarsfield 1611, X5016GCA, Ciudad Universitaria, Córdoba, Argentina.
[2] Address: Camino La Carrindanga Km 7, CC 717, 8000 Bahía Blanca, Provincia de Buenos Aires, Argentina. Tel.: +54 291 4861700.

http://dx.doi.org/10.1016/j.ces.2015.02.031
0009-2509/

## 1. Introduction

The oxidation of phenolic structures, as a means of decontamination of liquid effluents of textile, paper, and leather industries, is a very active research field. Research typically focuses on the study, application, and design of efficient catalysts for the degradation of phenolic compounds. In contrast to advanced oxidation processes and Fenton methods, the use of heme containing peroxidases as catalysts have the advantages of being highly efficient not only in the energetic requirements but also in the activation of the clean oxidant hydrogen peroxide. For example, under mild conditions (low temperature and peroxide concentration), peroxidases suppress the formation of peroxyl ($OOH^{\bullet}$) and alkoxyl ($OH^{\bullet}$) radicals and thus of $H_2O_2$ disproportionation. In addition, metal leaching, one of the main problems associated to iron-containing catalysts, is completely avoided using peroxidases. However, high cost, sensitivity to operational conditions, and incomplete oxidation of organic matter are the main caveats associated with the use of peroxidases for decontamination.

Hematin, an hydroxyl-ferri-protoporphyrin, is the oxidized form of free heme and serves as a robust cost-effective alternative to horseradish peroxidase (HRP). Hematin is released by blood-eating organisms and its characterization in aqueous solution is motivated mainly by antimalarial drugs development (De Villiers et al., 2007). The use of hematin as a catalyst for oxidative polymerizations of phenolic monomers and hydrogelation processes has been restricted due to its low solubility and aggregation at low pHs (Ryu et al., 2014; Sakai et al., 2010; Singh et al., 2001). Therefore, different functionalization strategies, including esterification with polyethylenglicol (PEGylatedhematin), amidation with methoxypolyethylene glycol amine and even its inclusion into micelles (Nagarajan et al., 2009; Ravichandran et al., 2012) have been attempted. Recent results by our group presented hematin as a promising alternative to HRP for decolorization reactions active at high peroxide concentrations (Córdoba et al., 2012a,b; Pirillo et al., 2010). Reports including hematin applications lack the mechanistic evaluation of catalytic action. However, several studies (Goh and Nam, 1999; Nam and Han, 2000; Stephenson and Bell, 2005; Traylor et al., 1993) demonstrated the existence of oxoperferryl π-cation radical species and oxoperferryl of synthetic meso-substituted iron porphyrins as the analogues of the key peroxidases intermediates, named as Compound I and Compound II, respectively. In comparison to synthetic meso-substituted iron porphyrins, hematin is a pyrrole-substituted compound showing a closer resemblance to heme-enzymes (see Fig. 1), which differ only in the coordination of the fifth position of the iron and lack of the surrounding proteic structure. Our UV/visible spectral inspection of hematin in alkaline $H_2O_2$ solutions revealed the existence of the oxoperferryl radical species as the main catalytic intermediary (Córdoba et al., 2012b).

The co-oxidation of phenols and 4-Aminoantipyrine (AAP) using $H_2O_2$ is a long established spectroscopic method for determination of phenol and of $H_2O_2$ in aqueous samples adapted to different flow injection modes (Mifune et al., 2003; Omuro Lupetti et al., 2004; Ribeiro et al., 2009). This method has been used for the determination of glucose, ethanol, lactate, cholesterol, peroxidase-based inmunoassays, and for monitoring of bioprocesses (Vojinovic et al., 2007). Indeed, a purple quinoneimine product of phenol and AAP was formed (Fig. 2). Originally, potassium ferricyanide in alkaline medium was applied as the catalyst (Emerson, 1943), however, current methods demonstrate different structures including HRP (Metelitza et al., 1991; Vojinovic et al., 2004), metal complexes (Omuro Lupetti et al., 2004; Rajendiran and Santhanalakshmi, 2006; Tang et al., 2002), and porphynes (Mifune et al., 2003; Odo et al., 2009) to be active as well. Moreover, the phenol/AAP/$H_2O_2$ reagents serve as a model system for testing peroxidase-like activities (Biava and Signorella, 2010; Mifuni et al., 2000; Odo et al., 2009).

The observation of oxygen evolution during reaction gives insight into peroxide decomposition. This reaction may have a negative impact on dye formation. First of all, peroxide decomposition consumes available $H_2O_2$. Secondly, generates highly reactive radicals such as $HOO^{\bullet}$ and $OH^{\bullet}$, which may attack not only substrates ($H_2O_2$, phenol, and AAP) and any of the intermediates products, but also the protein and porphyrin moieties of catalysts. These reactions produce oxygen as described by Pirillo et al. (2010). Pseudo-catalatic peroxide decomposition involving attack of $H_2O_2$ to Compound I is already known to be highly suppressed for HRP in the presence of organic substrates (Vlasits et al., 2010). However, as demonstrated by molecular modelling (Córdoba et al., 2012b), the coordination of $H_2O_2$ vs. phenol by the less specific oxoperferryl cation radical of hematin is highly feasible.

The objective of this work is the evaluation of hematin as a mimetic catalyst of HRP on the 4-aminoantipyrine/phenol co-oxidation reaction. This study was motivated not only by the potential application of hematin as a catalyst for the versatile 4-aminoantipyrine/phenol analytical method, but also for understanding hematin action over phenolic substrates. A kinetic model was applied for dye formation with HRP and hematin. Then, the rate constant values for the reactions were estimated by using a fitting procedure to experimental values and the differences encountered between the two catalysts are discussed. Inactivation routes were also incorporated at high oxidant concentrations. Furthermore, the peroxide decomposition reaction as a competitive route was

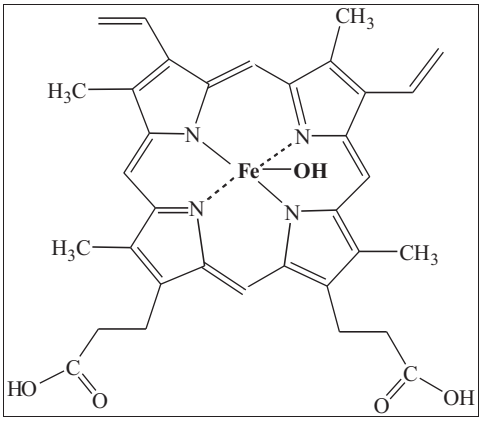


**Fig. 1.** Structure of hematin.

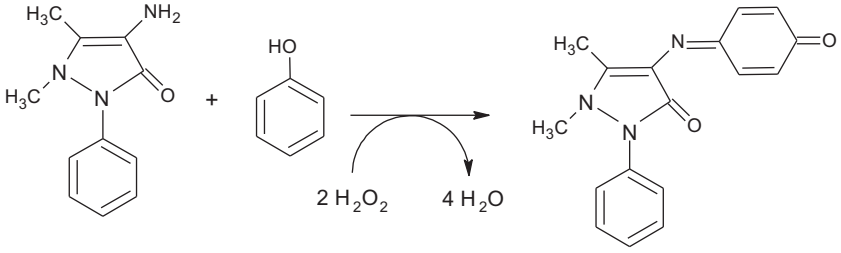


**Fig. 2.** Quinoneimine formation from phenol and 4-Aminoantipyrine (AAP).

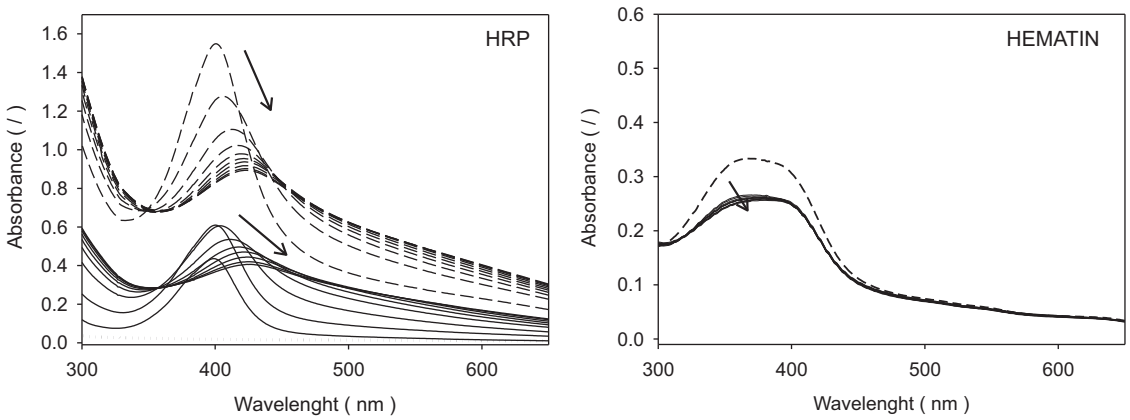


**Fig. 3.** Stacked UV/visible spectra of catalyzed phenol/$H_2O_2$ systems during the first 5 min of reaction. Initial concentrations were selected as follows: [Phenol]=8.35 mM; $[H_2O_2]_{HRP}$=0.3 and 3 mM (dashed line); $[H_2O_2]_{HEMATIN}$=17 mM; [HRP]=0.3 and 3 mg $l^{-1}$ (dashed line); [HEMATIN]=6 mg $l^{-1}$.

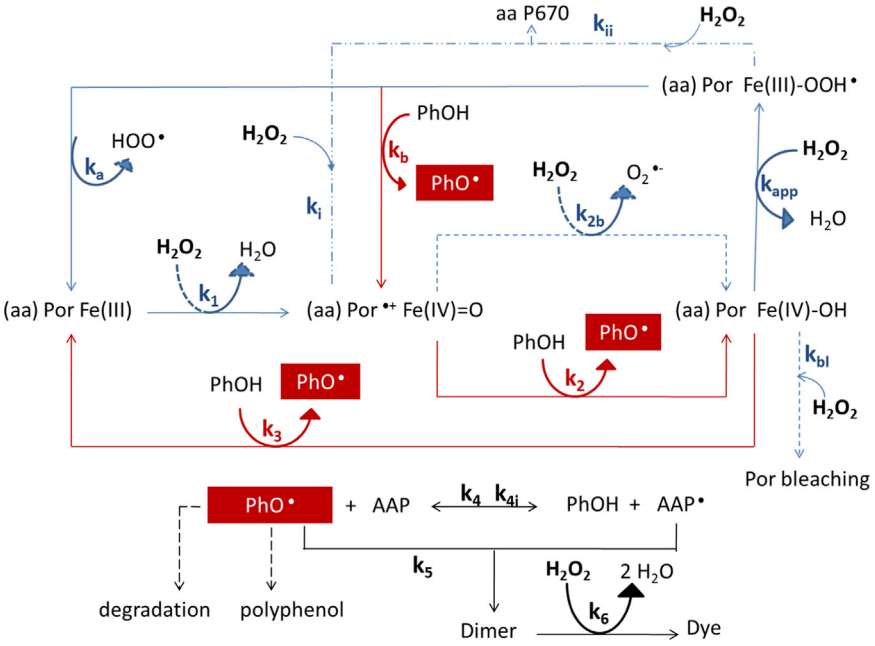


**Schema 1.** General reaction mechanism for dye formation including non-productive pathways. Continued arrows denote reaction mechanism of Nicell's model whereas dashed lines represent additional non-productive pathways considered for parametrization in the high $H_2O_2$ region.

analyzed. On the other hand, the high phenol excess applied in the reactions may promote its coupling or its oxidation by HOO• or OH• radicals. Therefore, the importance of these processes as side reactions to dye formation was checked throughout this study.

## 2. Modeling

### 2.1. Kinetic model

The kinetic mechanism of quinoneimine dye production was assumed to follow the steps of Nicell's model for HRP (Nicell and Wright, 1997), with modifications undertaken by Carvalho et al. (2006). The model consists of a series of six reactions and an inactivation route of three steps. The reactions involved are specified in Scheme 1 and described as follows: catalyst resting state (aa) Por Fe(III) ($E_0$) is oxidized by $H_2O_2$ to give the oxoperferryl π-cation radical (aa) $Por^{\bullet+}$ Fe(IV)=O or Compound I $E_I$ (reaction (1)—$k_1$), which in turn reduces back to resting state in two one-electron reductions. In this process, catalysts intermediaries $E_I$ and Compound II $E_{II}$ ((aa) Por Fe(IV)–OH) take one proton H•, respectively, from a phenol molecule (PhOH) generating phenoxy radicals (PhO•) (reactions (2) and (3)—$k_2$ and $k_3$). In the presence of AAP, phenoxy radicals transfer one electron to AAP in a reversible reaction (reaction (4)—$k_4$ and $k_{4i}$). AAP-radicals couple to phenoxy radicals (reaction (5)—$k_5$) and this structure (PhO · AAP) is oxidized by $H_2O_2$ to give the final product (reaction (6)—$k_6$). Due to the high phenol excess relative to AAP, the following reactions were considered as negligible: (1) oxidation of AAP by catalyst intermediaries $E_I$ and $E_{II}$ and (2) coupling of AAP radicals.

Nicell's model considers the reversible inactivation route of peroxidases through Compound III ($E_{III}$) ((aa) Fe(III)–OOH•) formation by attack of $H_2O_2$ to Compound II (reaction 7—$k_{aap}$). Then, $E_{III}$ undergoes decomposition with resting state restoration releasing OOH• (reaction 8—$k_a$) or it may be reduced to $E_I$ by phenol oxidation to phenoxy radical (reaction 9—$k_b$).

Mathematical description of this mechanism was achieved by mass balances of:

(1) Reaction substrates $H_2O_2$, PhOH and AAP:

$$\frac{d[H_2O_2]}{dt} = -k_1[E_0][H_2O_2] - k_6[\text{PhO}\cdot\text{AAP}][H_2O_2] - k_{app}[E_{II}][H_2O_2] \quad (1)$$

$$\frac{d[\mathrm{PhOH}]}{dt} = -k_2[E_I][\mathrm{PhOH}] - k_3[E_{II}][\mathrm{PhOH}] - k_b[E_{III}][\mathrm{PhOH}] + k_4[\mathrm{AAP}][\mathrm{PhO}^\bullet] - k_{4i}[\mathrm{AAP}^\bullet][\mathrm{PhOH}] \quad (2)$$

$$\frac{d[\mathrm{AAP}]}{dt} = -k_4[\mathrm{AAP}][\mathrm{PhO}^\bullet] + k_{4i}[\mathrm{AAP}^\bullet][\mathrm{PhOH}] \quad (3)$$

(2) All catalyst intermediaries (resting state $E_0$, Compound I $E_I$, Compound II $E_{II}$, and Compound III $E_{III}$):

$$\frac{d[E_0]}{dt} = -k_1[E_0][H_2O_2] + k_3[E_{II}][\mathrm{PhOH}] + k_a[E_{III}] \quad (4)$$

$$\frac{d[E_I]}{dt} = k_1[E_0][H_2O_2] - k_2[E_I][\mathrm{PhOH}] + k_b[E_{III}][\mathrm{PhOH}] \quad (5)$$

$$\frac{d[E_{II}]}{dt} = k_2[E_I][\mathrm{PhOH}] - k_3[E_{II}][\mathrm{PhOH}] - k_{app}[E_{II}][H_2O_2] \quad (6)$$

$$\frac{d[E_{III}]}{dt} = k_{app}[E_{II}][H_2O_2] - k_a[E_{III}] - k_b[E_{III}][\mathrm{PhOH}] \quad (7)$$

and

(3) Reaction intermediaries $\mathrm{PhO}^\bullet$, $\mathrm{AAP}^\bullet$, and $\mathrm{PhO}\cdot\mathrm{AAP}$:

$$\frac{d[\mathrm{PhO}^\bullet]}{dt} = k_2[E_I][\mathrm{PhOH}] + k_3[E_{II}][\mathrm{PhOH}] - k_4[\mathrm{AAP}][\mathrm{PhO}^\bullet] + k_{4i}[\mathrm{AAP}^\bullet][\mathrm{PhOH}] + k_b[E_{III}][\mathrm{PhOH}] - k_5[\mathrm{PhO}^\bullet][\mathrm{AAP}^\bullet] \quad (8)$$

$$\frac{d[\mathrm{AAP}^\bullet]}{dt} = k_4[\mathrm{AAP}][\mathrm{PhO}^\bullet] - k_{4i}[\mathrm{AAP}^\bullet][\mathrm{PhOH}] - k_5[\mathrm{PhO}^\bullet][\mathrm{AAP}^\bullet] \quad (9)$$

$$\frac{d[\mathrm{PhO}\cdot\mathrm{AAP}]}{dt} = k_5[\mathrm{PhO}^\bullet][\mathrm{AAP}^\bullet] - k_6[\mathrm{PhO}\cdot\mathrm{AAP}][H_2O_2] \quad (10)$$

Mass balance of the product Dye was also included for simulation of its profile:

$$\frac{d[\mathrm{Dye}]}{dt} = k_6[\mathrm{PhO}\cdot\mathrm{AAP}][H_2O_2] \quad (11)$$

The resulting model is comprised of (11) differential equations and (10) kinetic rate expressions. Formation of inactive state P670 from $E_I$ and $E_{III}$ was added to this model in order to explain HRP catalyzed dye profiles at high $H_2O_2$ initial concentrations (Section 4.3) and are specified in Scheme 1 as doted-dashed lines. Mass balance of $E_{P670}$ was added and mass balances of $H_2O_2$, $E_I$ and $E_{III}$, were modified accordingly as follows:

$$\frac{d[E_{P670}]}{dt} = k_i[E_I][H_2O_2] + k_{ii}[E_{III}][H_2O_2] \quad (12)$$

$$\frac{d[H_2O_2]}{dt} = -k_1[E_0][H_2O_2] - k_6[\mathrm{PhO}\cdot\mathrm{AAP}][H_2O_2] - k_{app}[E_{II}][H_2O_2] - k_i[E_I][H_2O_2] - k_{ii}[E_{III}][H_2O_2] \quad (13)$$

$$\frac{d[E_I]}{dt} = k_1[E_0][H_2O_2] - k_2[E_I][\mathrm{PhOH}] + k_b[E_{III}][\mathrm{PhOH}] - k_i[E_I][H_2O_2] \quad (14)$$

$$\frac{d[E_{III}]}{dt} = k_{app}[E_{II}][H_2O_2] - k_a[E_{III}] - k_b[E_{III}][\mathrm{PhOH}] - k_{ii}[E_{III}][H_2O_2] \quad (15)$$

Thus, the modified model for HRP at high peroxide concentrations comprises Eqs. (2)–(4), (6) and (8)–(15). On the other hand, porphyrin bleaching from intermediary Por Fe(IV)–OH and reduction of $\mathrm{Por}^{\bullet+}$ Fe(IV)=O state by $H_2O_2$, were added as additional routes in case of hematin catalysis at high $H_2O_2$ conditions. These reactions are represented with dashed lines in Scheme 1. Mass balance of the bleached porphyrin $E_{bl}$ was incorporated:

$$\frac{d[E_{Bl}]}{dt} = k_{Bl}[E_{II}][H_2O_2] \quad (16)$$

Besides, mass balances of $H_2O_2$, $E_I$ and $E_{II}$ were replaced by

$$\frac{d[H_2O_2]}{dt} = -k_1[E_0][H_2O_2] - k_6[\mathrm{PhO}\cdot\mathrm{AAP}][H_2O_2] - k_{app}[E_{II}][H_2O_2] - k_{2b}[E_I][H_2O_2] - k_{Bl}[E_{II}][H_2O_2] \quad (17)$$

$$\frac{d[E_I]}{dt} = k_1[E_0][H_2O_2] - k_2[E_I][\mathrm{PhOH}] + k_b[E_{III}][\mathrm{PhOH}] - k_{2b}[E_I][H_2O_2] \quad (18)$$

$$\frac{d[E_{II}]}{dt} = k_2[E_I][\mathrm{PhOH}] - k_3[E_{II}][\mathrm{PhOH}] - k_{app}[E_{II}][H_2O_2] + k_{2b}[E_I][H_2O_2] - k_{Bl}[E_{II}][H_2O_2] \quad (19)$$

Thereby, modified model for hematin at high peroxide concentrations comprises Eqs. (2)–(4), (7)–(11) and (16)–(19).

Initial concentrations of reaction substrates $H_2O_2$, PhOH, and AAP, as well as of catalyst resting state $E_0$, were set according to experimental conditions. Reaction products and all reaction and catalysts intermediaries were set to zero. In contrast to Carvalho et al. (2006), no steady-state conditions of catalysts intermediaries were assumed in this work. Preliminary simulations indicated that $E_0$ and $E_{III}$ concentrations varied considerably during reaction because the recovery to resting state was much slower than $E_{III}$ formation, which resulted in an accumulation of the latter with reaction time. Finally, the non-catalytic $H_2O_2$ disproportionation (Carvalho et al., 2006) was not included since oxygen did not evolve during reaction (see Fig. 4).

### 2.2. Parameter estimation

Sensitive kinetic rate constants were estimated based on experimental data using the parameter estimation tool of gPROMS 3.2 (general PROcess Modeling System, Process Systems Enterprise Ltd., London, United Kingdom). First, the mathematical model was implemented using this software. Then, the parameter estimation problem was solved using the parameter estimation tool of gPROMS. The built-in solver MAXLKHD was implemented, which performed the parameter estimation following a maximum likelihood approach (PSE, 2004). The standard built-in solver DASOLV was used for integration of the model equations and their sensitivity equations for the parameter estimation, which is based on variable time step/variable order backward differentiation formulae (BDF). The accuracy of the models obtained was analysed by the goodness-of-fit test performed by the parameter estimation tool of gPROMS. If the sum of weighted residuals was less than the 95% chi-square value ($\chi^2$ (95%)), a good fit was obtained. The software offers the possibility of selecting different variance models for the measured data. From the available options (PSE, 2004), the constant relative variance model ($\sigma^2 = w^2 z^2$, being $\sigma$the standard deviation, $z$ the model prediction of the measured quantity and $w$ a variance model parameter) was chosen for HRP catalyzed systems and the heteroscedastic variance model ($\sigma^2 = w^2(z^2)^\gamma$, $w$ and $\gamma$ variance model parameters) for hematin catalyzed systems. Parameters $w$ and $\gamma$ were determined by the parameter estimation procedure and initial guesses were set according to the average of the standard deviations of experimental measurements. The most sensitive rate constants were ranked by performing a global sensitivity analysis on the dynamic model. A total of thirty simulations were carried out for every catalyst at the initial guess value of every rate constant and at its ±20% variation, fixing in time all remaining constants values to initial guesses (Table 1). Simulated conditions were $[\mathrm{Phenol}]_0$: 8.35 mM, $[\mathrm{AAP}]_0$: 0.107 mM, $[H_2O_2]_0$: 0.3 mM, and $[E_0]$: 0.3 mg $l^{-1}$ for HRP, whereas for hematin were $[H_2O_2]_0$: 17.3 mM and $[E_0]$: 6.0 mg $l^{-1}$.

Assuming that the catalytic steps 1 to 3 are rate-controlling and considering global reaction stoichiometry (Fig. 2) i.e. $r_{PhOH}=r_{Dye}$, the following mathematical expression was applied for a data-based setting of initial guesses for the estimation of $k_1$ and $k_3$:

$$-r_{Dye,0}=\frac{E_T}{(1/k_1)(1/H_2O_2)_0+(1/k_3)(1/PhOH)_0} \quad (20)$$

Initial rates of dye formation were plotted vs. initial $H_2O_2$ concentration in a reciprocal fashion and the data were fitted to a linear curve, whose slope corresponds to $(E_T\,k_1)^{-1}$ and its intercept to $(E_T\ k_3\ [PhOH]_0)^{-1}$, $E_T$ being the applied catalyst concentration. Eq. (20) was obtained after combination of the mass balances of PhOH, $E_0$, $E_I$, and $E_{II}$ assuming that: (1) $E_T=E_0+E_I+E_{II}$; (2) steady state for catalyst intermediaries; and (3) $k_2 \gg k_3$ (Dunford, 1999). Initial guesses of the remaining model constants were set according to the values optimized by Carvalho et al. (2006) for an HRP catalyzed system. Initial guess for $k_2$ were set at 10 times the initial guess for $k_3$ for both catalytic systems (Dunford, 1999). The guess value of $k_i$ was taken from Hernández-Ruiz et al. (2001) and the guess value of $k_{ii}$ from Adediran and Lambeir (1989). The guess value of $k_{bI}$ was varied in different estimation trials around the value published by Cunningham et al. (2001). The initial guess of $k_{2b}$ was set as equal to the rate constant value of the competitive route, $k_2$.

A time of 17 s was added to the first absorbance measurement of every run because of the delay in data collection associated to sample manipulation. Hematin catalyzed time curves were corrected by deducing absorbance residual of hematin at 510 nm ($\lambda$), according to the hematin calibration curve; $\lambda=0.008$ [hem]+0.023; [hem] being the hematin concentration of every run in mg $l^{-1}$. In order to avoid absorbance interference by the produced polyphenolic material, HRP catalyzed time curves were loaded in gPROMS for the parameter estimation problem until the time of slope-change-point was reached (see Section 3.2).

## 3. Experimental

### 3.1. Materials

Hematin porcine ($M_w$=633.49) from Sigma Co. (San Luis, U.S.A.) and HRP ($M_w$: 41,000 Da) from Amano Inc. (Elgin, U.S.A.) were employed as provided. Hematin was applied from two different batches. Phenol and AAP were obtained from Tetrahedron (Godoy Cruz, Argentina) and Carlo Erba Reagents (Val de Reuil, France), respectively. 30vol hydrogen peroxide solution was obtained from Apotarg S.R.L. Laboratories (Córdoba, Argentina). All other chemicals were of analytical grade.

### 3.2. Kinetic assay

A volume of 500 mg $l^{-1}$ HRP raw solutions were prepared in $KH_2PO_4$/NaOH buffer at 0.1 M, pH 7 and stirred 30 min before use. Hematin was dissolved in NaOH 0.01 M and stirred 15 min before use at concentrations of 324 mg $l^{-1}$ and 1050 mg $l^{-1}$, for batch 1 and batch 2, respectively. 3 mM AAP and 140 mM phenol raw solutions were prepared in $KH_2PO_4$ buffer 0.1 M, pH 7. Reactions were carried out in a final volume of 3 ml, in a plastic cuvette at room temperature. AAP and phenol concentrations were 0.11 mM and 8.35 mM, respectively, in all experimental runs. Aliquots of the $KH_2PO_4$/NaOH buffer (0.1 M, pH 7), catalyst solution, AAP, and phenol solutions were added shortly before reaction in order to reach the required final concentrations. For parameter estimation purposes, a total of 15 runs for HRP and 20 runs for hematin were conducted varying the initial $H_2O_2$ concentration (0.26–17.3 mM for HRP and 1.73–300.2 mM for hematin) and catalyst concentration (0.3–1.7 mg $l^{-1}$ for HRP and 0.3–18.8 mg $l^{-1}$ for hematin). Each run was performed in triplicate. Reaction was initiated by one-step addition of $H_2O_2$ as a diluted solution in $KH_2PO_4$ buffer 0.1 M, pH 7. Upon addition of $H_2O_2$, the cuvette was capped and inverted three times prior to being placed in the spectrophotometer. A Perkin-Elmer Lambda 35 spectrophotometer (Massachusetts, U.S.A) was used for all UV/Visible measurements. Colour formation was measured during 300 s of reaction, at 510 nm absorbance and at 1 s intervals. For stacked spectra measurements, the absorbance region 300–800 nm was collected every 30 s. Molar absorptivity of the quinoneimine dye was determined assuming following: (1) dye was generated until completed conversion of limiting substrate AAP, and (2) the absorbance value to this point correspond to the slope-change-point of dye profiles catalyzed by HRP. Thus, a total of 27 absorbance values were collected from dye profiles and averaged in order to obtain the extinction coefficient value at 510 nm ($13473 \pm 296\ M^{-1}\ cm^{-1}$). Initial reaction rates presented in Fig. 5 were calculated by $(d[Dye]/dt)_{t=0}$.

**Table 1**
Initial guesses, optimized and reference rate constant values of model Eqs. (1)–(11).

| [$mM^{-1}\ s^{-1}$] | Initial guess value | | Optimized value | | Reference value | |
|---|---|---|---|---|---|---|
| | HRP | Hematin | HRP | Hematin | HRP | Iron porphirins |
| $k_1$ | $1.70 \times 10^3$ | $1.70 \times 10^{-2}$ | $1.05 \times 10^4 \pm 2.4 \times 10^3$ | $1.14 \times 10^{-2} \pm 5.0 \times 10^{-4}$ | $10^3$–$10^4$[c,d,e] | $10^{-1}$[f] |
| $k_2$ | 10 $k_3$ | 10 $k_3$ | $2.4 \times 10^2$[b] | 3.0 $10^{-1}$[b] | $2.8 \times 10^3$[d] | – |
| $k_3$ | $2.4 \times 10^1$ | $3.0 \times 10^{-2}$ | $1.7 \times 10^1 \pm 2.6 \times 10^{-1}$ | $7.58 \times 10^{-2} \pm 1.2 \times 10^{-2}$ | $3.2 \times 10^2$[d] | $10^{-1}$[f] |
| $k_4$ | $1.55 \times 10^3$[a] | | $1.55 \times 10^3$[b] | | – | – |
| $k_{4i}$ | $1.63 \times 10^{-5}$[a] | | $1.63 \times 10^{-5}$[b] | | – | – |
| $k_5$ | $3.42 \times 10^5$[a] | | $3.42 \times 10^5$[b] | | – | – |
| $k_6$ | $3.35 \times 10^2$[a] | | $3.35 \times 10^2$[b] | | – | – |
| $k_{app}$ | $1.13 \times 10^{-1}$[a] | | $7.5 \times 10^{-3} \pm 9.4 \times 10^{-4}$ | $3.05 \times 10^{-3} \pm 4.8 \times 10^{-4}$ | $2.5 \times 10^{-2}$[c] | $10^{-1}$[f] |
| $k_a$ [$s^{-1}$] | $8.09 \times 10^{-4}$[a] | | $1.5 \times 10^{-2} \pm 2.9 \times 10^{-3}$ | $2.24 \times 10^{-3} \pm 7.4 \times 10^{-5}$ | $2 \times 10^{-3}$[c] | |
| $k_b$ | $5.35 \times 10^{-6}$[a] | | $5.35 \times 10^{-6}$[b] | | $9.5 \times 10^{-4}$[d] | - |
| Initial guess of $\sigma^2$ | | | $0.10^2$ [Dye]$^2$ | $0.010^2$ [Dye]$^{0.5*2}$ | | |
| Optimized $\sigma^2$ | | | $0.11^2$ [Dye]$^2$ | 0.018 [Dye]$^{0.4*2}$ | | |
| Weighted residuals | | | 1774.7 | 12,549 | | |
| $\chi^2$ (95%) | | | 1911.1 | 13,200 | | |

[a] Taken from Carvalho et al. (2006).
[b] Taken as fixed during rate constant estimation procedure.
[c] Vlasits et al., 2010.
[d] Nicell et al., 1997.
[e] Dunford, 1999.
[f] Cunningham et al., 2001.

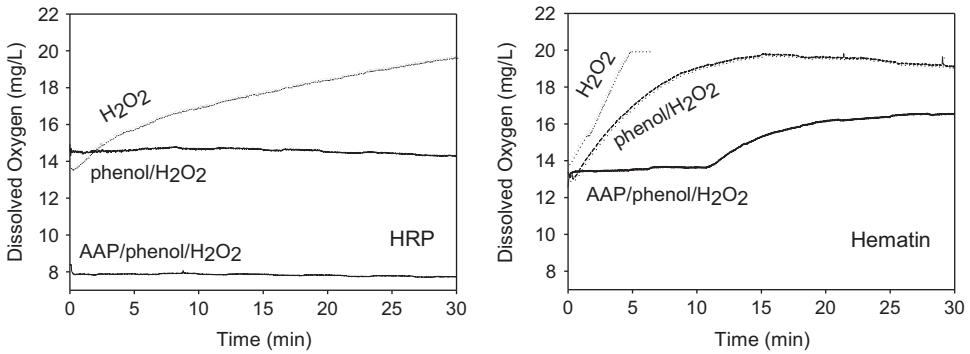


**Fig. 4.** Dissolved oxygen evolution in catalyzed reacting systems AAP/phenol/$H_2O_2$, phenol/$H_2O_2$ and $H_2O_2$. Hematin/HRP concentrations were at 6 mg $l^{-1}$ whereas initial substrates concentrations were as follows: AAP: 0.11 mM, phenol: 8.35 mM and $H_2O_2$, 17 mM.

### 3.3. Dissolved oxygen measurement

Dissolved oxygen profiles were measured with a Pasco Pasport Dissolved Oxygen Sensor model PS-2108 (California, U.S.A.). Reactions were carried out with magnetic stirring at 25 °C on a final volume of 50 ml in $KH_2PO_4$/NaOH buffer at 0.1 M, pH 7. Reaction was initiated after sensor stabilization by one-step addition of $H_2O_2$. Selected experimental conditions were as follows: catalyst concentration: 6 mg/l; $H_2O_2$concentration: 17 mM; phenol concentration: 8.35 mM (when present); and AAP concentration: 0.11 mM (when present). The measurement was continuous during 300 s.

## 4. Results and discussion

### 4.1. Inspection of side reactions to dye formation

Product dye spectra (not shown) presented $\lambda_{max}$ values in accordance with published data (Fiamegos et al., 2002; Li et al., 2011; Rajendiran and Santhanalakshmi, 2006), thus confirming formation of the target dye for both catalysts. Absorbance time profiles of HRP-catalyzed systems were nearly straight until a value of $1.44 \pm 0.02$, which was assumed as the reaction completion point, due to AAP depletion. However, absorbance continued increasing thereafter at a slow rate dependent on the initial $H_2O_2$ concentration. Moreover, this second slope region was absent whenever $H_2O_2$ was limiting and in hematin catalyzed systems reaching reaction completion. Fig. 3 shows stacked spectra for systems without AAP. The spectral evolution for the HRP systems corresponds to accumulation of phenoxy radicals followed by recombination with formation of polyphenolic products (Akkara et al., 2000; Ghosh Datta et al., 2012; Reihmann and Ritter, 2006). Indeed, the typical brown precipitate corresponding to polyphenolic products was observed. Hematin spectrum (dashed line on Fig. 3-hematin) was in line with those observed by Egan et al. at neutral pH (De Villiers et al., 2007). After $H_2O_2$ addition, an hypochromic shift of the Soret band of hematin occurred due to Compound I formation (Córdoba et al., 2012b; Dunford, 1999). Then, a slight drop in the 350 nm region was observed. Thus, phenoxy radical recombination was not detected in the system and no precipitates were observed after reaction. Hematin hydroperoxides systems are known to produce peroxyl radicals (Kalyanararnan et al., 1983; Van Der Zee et al., 1996). Peroxyl radicals are in acid-base equilibrium with super oxide radicals $O_2^{\bullet -}$, that are rapidly reacting with phenoxyl radicals by addition, rearrangement and possibly ring opening for aromatics (René et al., 2010; Stephenson and Bell, 2005). Thus, phenoxy radical decomposition rather than phenoxy coupling is suggested to occur with hematin.

Higher concentrations of both $H_2O_2$ and HRP promote accumulation of phenoxy radicals (see Fig. 3) and thus, phenoxy–phenoxy pairing over phenoxy-AAP combination. Therefore, absorbance values at the AAP depletion point should have varied in HRP with changing $H_2O_2$ and HRP concentration and with respect to maxima values reached with hematin systems. However, this was not the case. It can be cautiously assumed that phenoxy–phenoxy pairing becomes important only when AAP is nearly 100% converted and can be neglected as a side route in the proposed model.

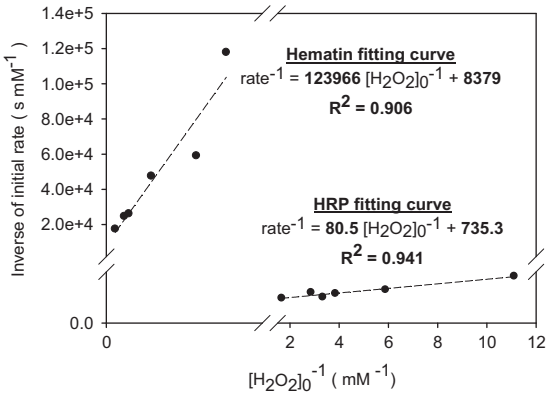


**Fig. 5.** Initial rate vs. initial peroxide concentration at fixed catalyst concentration in reciprocal fashion (see Section 3 for reaction conditions).

Fig. 4 shows oxygen profiles for three different catalyzed reacting systems: $H_2O_2$; $H_2O_2$/phenol; and $H_2O_2$/phenol/AAP. The oxygen evolution observed, when $H_2O_2$ was applied as the unique substrate with both catalysts, correspond to catalase (Hernández-Ruiz et al., 2001) or pseudo-catalase activities (Vlasits et al., 2010). In the phenol/$H_2O_2$ and AAP/phenol/$H_2O_2$ system no oxygen evolved by HRP catalysis. Thus, phenol inhibited the catalatic reaction of HRP. On the contrary, there was an important oxygen evolution with hematin in the phenol/$H_2O_2$ system, corresponding not only from a catalase or pseudo-catalase pathway taking place in competition with phenol oxidation, but also from attack of peroxyl radicals to phenoxy radicals (Pirillo et al., 2010). This last assumption is consistent with the spectral evolution observed in Fig. 3 and the lack of polyphenol production.

There was a strong selection for $H_2O_2$ coordination with hematin, but in the case of HRP, only the first step of $H_2O_2$ coordination to generate Compound I was favoured. The coordination of phenolic compounds in Compound I and Compound II was always favoured. Therefore, spontaneous decay in Compound III and generation of oxygen was difficult. The reaction with phenols was the preferred path with HRP. The Compound III of HRP may decay to Ferrous $Fe^{+2}$–H and later to the native enzyme; but only if it formed first from Compound II (Dunford, 1999) (see Scheme 1). Otherwise, the other pathway is to lose $HO_2^{\bullet}$ that,

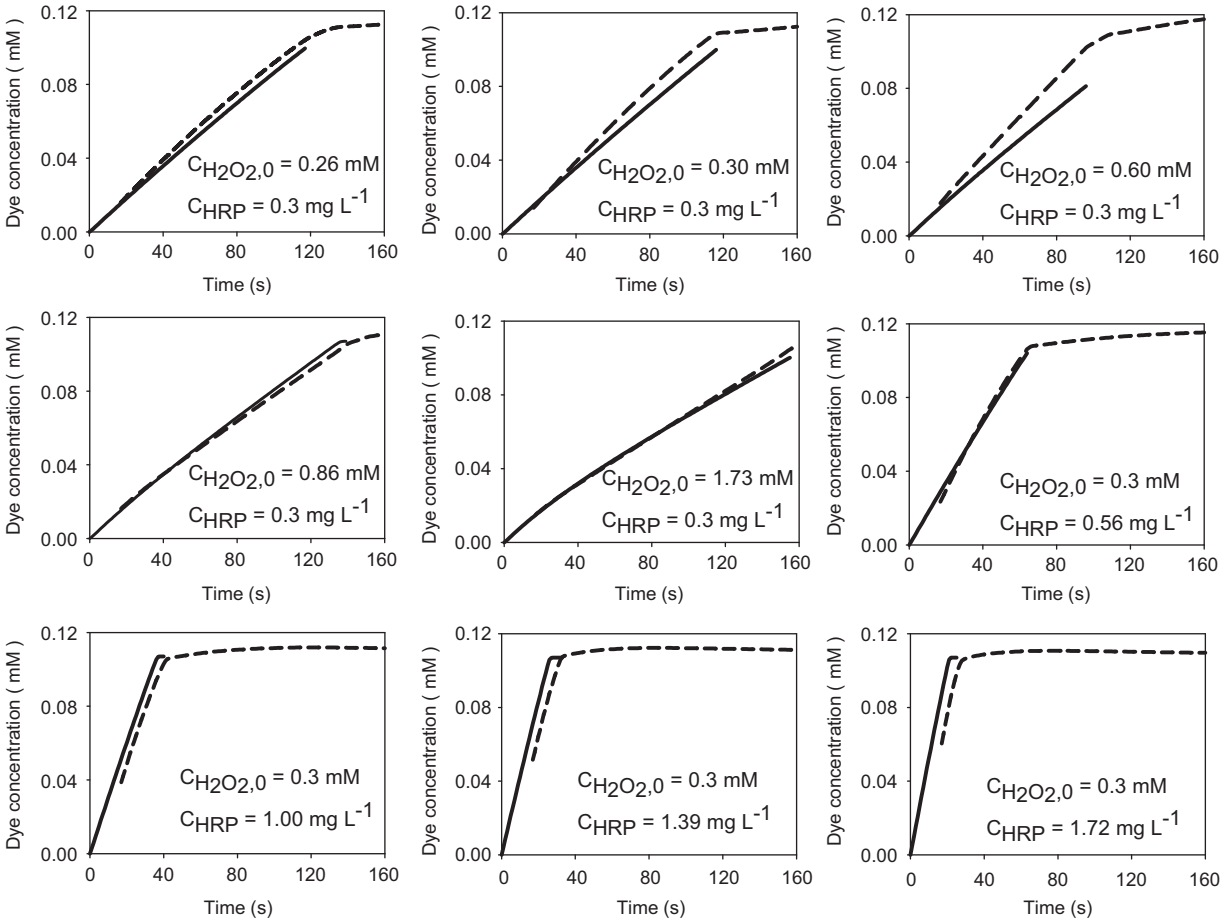


**Fig. 6.** Experimental (short dash lines) and modelled (continuous lines) dye concentration profiles at varying concentration of hydrogen peroxide and HRP applied for the rate constant estimation procedure.

in excess of PhOH, may react with it and generate a radical PhO$^{\bullet}$ and $H_2O_2$. Now, it seems that in the case of hematin, the loss of $O_2$ is more probable through the Compound III decay instead of through $H_2O_2$ coordination to Compound I.

When AAP was added to the system, oxygen evolution was suppressed by hematin. However, oxygen evolved when hematin was present and AAP was totally converted, thus resembling the oxygen profile of the previously described phenol/$H_2O_2$ system. Therefore, it is highly likely that phenoxy radicals transfer an electron to AAP instead of being oxidized by peroxyl radicals. Therefore, the postulated model for dye formation can be evaluated with hematin as catalyst, at least in a first instance, without addition of secondary routes.

### 4.2. Rate constants estimation

Initial guess values of model parameters are critical for the estimation procedure and the accuracy of the optimal solution found therein. Therefore, whenever possible, initial guess values should be taken from experimental findings. Fig. 5 shows data of initial rates vs. peroxide concentration in a reciprocal fashion of data pairs. The linear dependency observed for both catalytic systems confirmed that the catalytic cycle was rate-controlling. The fitting procedure to a linear curve (see Eq. (20)) provided initial guess values for $k_1$ and $k_3$ (see Table 1). Preliminary estimation trials resulted in a statistically accurate model; however, most rate constants were statistically insignificant having standard deviations much higher than their estimated values. Therefore, every rate constant was subjected to a sensitivity analysis. The relevant kinetic constants that resulted were $k_1$, $k_3$, $k_{app}$, and $k_a$. Model outputs resulted most sensitive to changes in $k_3$ and $k_{app}$ at the end of reaction, whereas $k_1$ was significant from the beginning. Variations of the remaining constants $k_2$, $k_4$, $k_{4i}$, $k_5$, $k_6$, and $k_b$ did not produce any appreciable changes in the dye profiles. In light of this information, the estimation procedure was re-conducted for every catalyst only for the relevant rate constants, fixing remaining rate constants at their guess values. Table 1 provides the optimized rate constant values, the optimized variance model and the sum of weighted residuals relative to the $\chi^2$ (95%). Figs. 6 and 7 illustrate the agreement between experimental and modelled data. Standard deviations of the estimated constants are acceptable and in line with the sensitivity analysis results.

Rate constant of HRP-Compound I formation was estimated within the range of reference values. However, the rate constant corresponding to native state regeneration ($k_3$) resulted somewhat lower. The estimated values for constants $k_{app}$ and $k_a$, corresponding to the reversible inactivation pathway initiated by attack of $E_{II}$ intermediate by $H_2O_2$, resulted in a Compound III formation step rather lower than published data and its decomposition step to native state somewhat higher. However, the overall reaction rate of the pathway was in accordance to published literature. Moreover, the estimated values of $k_{app}$ and $k_a$ were also similar for HRP and hematin. According to the kinetic model, the ratio $k_3$[Phenol] to $k_{app}[H_2O_2]$ controlled the reaction flux distribution from dye formation to peroxide decomposition, and this ratio was 124 times higher for the enzyme at equal phenol to peroxide molar ratios.

Looking at the concentration ratio $H_2O_2$ to HRP in terms of mM l $mg^{-1}$, three ranges of analysis were identified for the proposed mechanism and its impact in the fitting of experimental

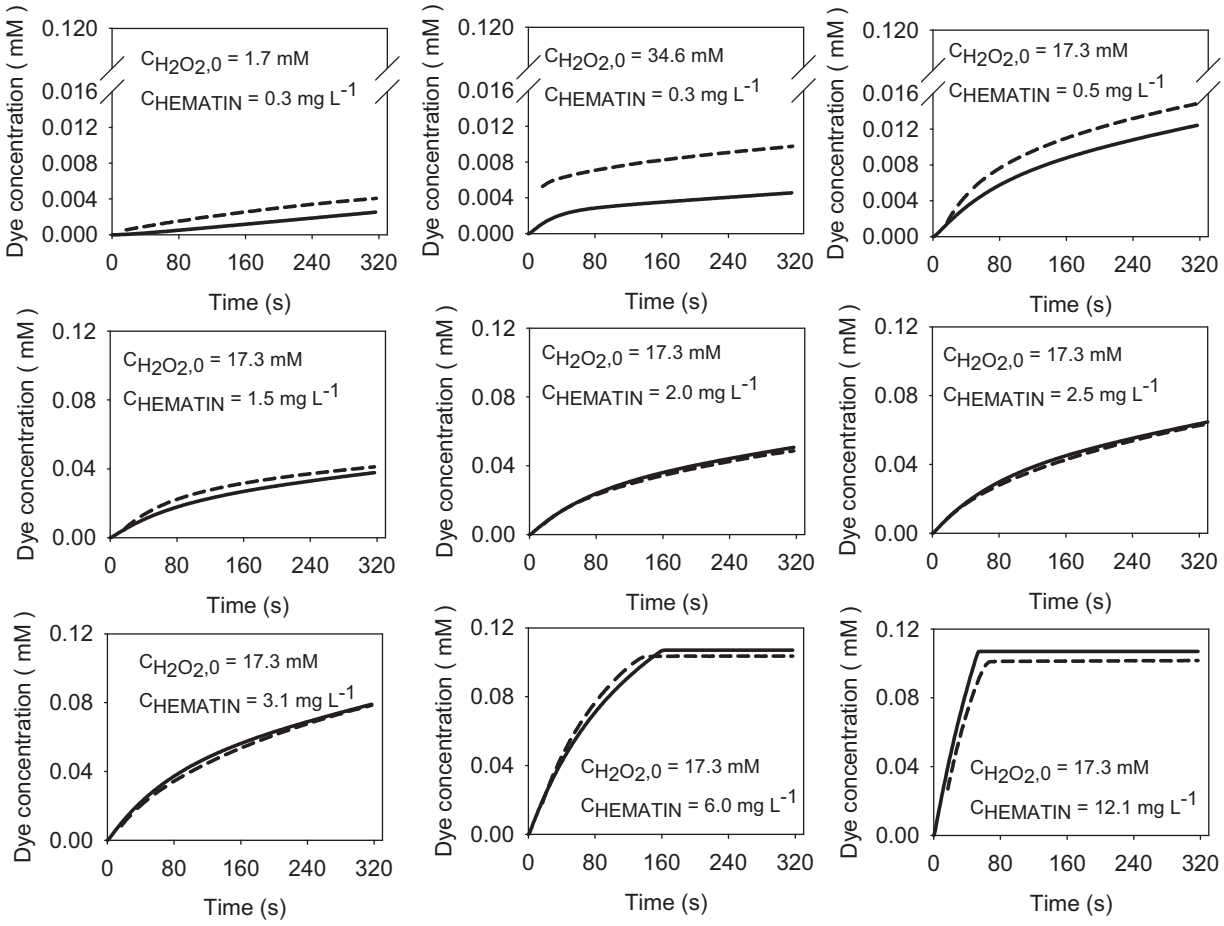


**Fig. 7.** Experimental (short dash lines) and modelled (continuous lines) dye concentration profiles at varying concentration of hydrogen peroxide and hematin applied for the rate constant estimation procedure.

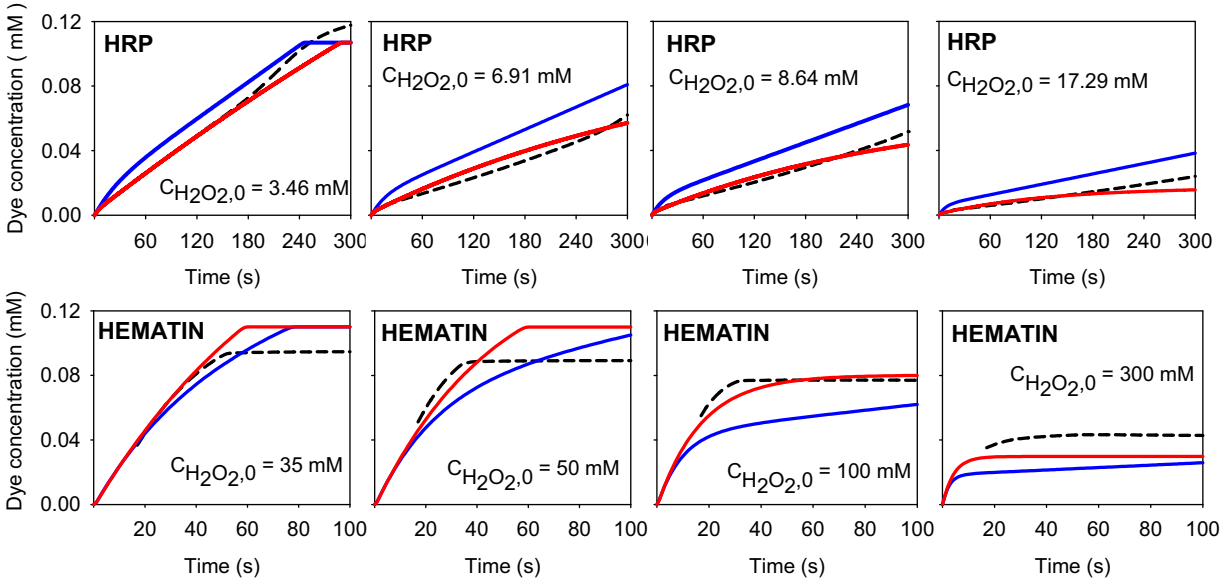


**Fig. 8. (black and white for printing version):** Experimental (short dash lines) and modelled (continuous lines) dye profiles of HRP/hematin catalyzed systems at high $H_2O_2$ concentrations. Black line: from original model. Gray lines: estimation of modified model according to Schema 1. $C_{HRP}$=0.3 mg $l^{-1}$ and $C_{hematin}$=5.95 mg $l^{-1}$. **(coloured version for the web):** experimental (short dash lines) and modelled (continuous lines) dye profiles of HRP/hematin catalyzed systems at high $H_2O_2$ concentrations. Blue line: from original model. Red lines: Estimation of modified model according to Schema 1. $C_{HRP}$=0.3 mg $l^{-1}$ and $C_{hematin}$=5.95 mg $l^{-1}$.

data. Below a concentration ratio of 1 and above a concentration ratio of 2, the model fit experimental data. For example, when enough HRP was present or at an excess of $H_2O_2$, the model adequately fit the data. But, when the concentrations were intermediate, underestimation of dye formation occurred. There was a compensation effect that was not adequately included or the

deactivation constant and mechanism were different in this concentration range, suggesting that a deactivation reaction was overrepresented here (see Fig. 6). Considering HRP-Compound III a resonance structure is possible:

$$H^+ – Fe^{III} – O_2^- \rightarrow H^+ – Fe^{II} – O_2$$

Other mechanism involves the formation of superoxide:

$$H^+ – Fe^{IV} = O + H_2O_2 \rightarrow [Fe^{III}, H_2O, HO_2^{\bullet}] \rightarrow H^+ – Fe^{III} – O_2^- + H_2O$$

Now, if deactivation was overrepresented with HRP in the model, the real situation of higher than modeled dye formation could be assigned to a reaction only operative in this range of ratio $H_2O_2$ to HRP that regenerated ferric enzyme. When hydrogen peroxide/HRP concentrations ratio was higher than 2, the deactivation was fully operative and this regeneration of native enzyme was no longer operative to overcome the deactivation reaction. At low hydrogen peroxide concentration, peroxide was used in the first step but there was a strong affinity of the HRP to phenol and the impact of the reaction presented above was minor. At intermediate concentrations, deactivation was not as important and the above reaction may have added active enzyme to produce more dye due to the regeneration of active enzyme more efficiently.

On the other hand, the model presented a tendency of underestimation of hematin catalyzed dye profiles with the increase on the peroxide to hematin concentration ratio being remarkable at high values (see first line in Fig. 7). It seems that whether deactivation is overrepresented or the regeneration route was not properly described by the model. A higher than proposed order of reaction of peroxide in the resting state activation reaction or even in any regeneration step may be involved. This supposition implies that more than one peroxide molecule would coordinate to ferric enzyme as postulated by Akkara et al. (2000)) (see Section 4.3).

A question arises whether the catalytic intermediates involved in the proposed model for HRP are also applicable to hematin. Traylor et al. (1993) postulated that a heterolytic rather than homolytic cleavage of the O–O bond of $H_2O_2$ occurred with concomitant oxoperferryl π-cation radical formation upon reaction on iron(III) tetrakis(pentafluorophenyl)porphyrin chloride ($F_{20}$TPPFeCl). However, the existence of the oxoperferryl species on those reacting systems arises from attack of a second molecule of peroxide on the oxoperferryl π-cation radical and the importance of this reaction relative to an attack of a reducing substrate appear to lie on the electronic withdrawing effect of the substituent of the porphyrin (Goh and Nam, 1999; Traylor et al., 1993). More specifically, Cunningham et al. (2001) estimated rate constant values for the formation of the oxoperferryl π-cation radical and the resting state regeneration from the oxoperferryl state upon attack of hydrogen peroxide of the system $F_{20}$TPPFeCl–$H_2O_2$–cyclooctene in a solvent mixture $CH_3OH$–$Cl_2H_2$. They also estimated the rate constant value of resting state regeneration from the oxoperferryl state upon attack on 2,4-methoxyphenol. These values are shown in Table 1. Nevertheless, they did not mention any formation of an analogue of Compound III on the pathway involved on resting state regeneration upon peroxide attack of the oxoperferryl species.

### 4.3. Model extrapolation at high $H_2O_2$ concentrations

High $H_2O_2$ concentrations may be involved in the application of HRP/hematin in effluent decolorization treatments. On the other hand, in light of the results obtained in this study, productive hematin catalyzed dye formation needs higher $H_2O_2$ concentrations in order to overcome the much lower $k_1$ constant value for resting state activation. However, the reaction flux through the reversible inactivation pathway via $E_{II}$ intermediate becomes important. Simulation results conducted by Vojinovic et al. (2007) on HRP catalyzed dye profiles using Nicell's model gave poor fitting to experimental data at initial $H_2O_2$ concentrations higher than 3.7 mM. Thus, additional routes may become important at high $H_2O_2$ concentrations (Adediran and Lambeir, 1989; Hernández-Ruiz et al., 2001), e.g., formation of inactive P-670 state in case of HRP.

Simulated dye profiles by HRP catalysis with rate constants values in Table 1 gave a clear overestimation compared to experimental profiles in the $H_2O_2$ range of 3.46 to 17.29 mM (see Fig. 8). Therefore, as described in Scheme 1, the following routes were incorporated to the original model: (1) formation of *P*-670 state from Compound I state ($k_i$) and (2) formation of *P*670 state from Compound III state ($k_{ii}$). A rate constant estimation procedure for $k_i$ and $k_{ii}$, fixing all remaining constants to their optimal values of Table 1, yielded an inaccurate solution. Therefore, inactivation rate constants, $k_{app}$ and $k_a$, were also re-evaluated within the procedure mentioned above. Results are provided in Table 2 and Fig. 8. In light of the optimized rate constant values, formation of inactive state *P*-670 from Compound III emerged as the unique formation route. Model dye profiles approached closer to experimental data, whereas underestimation was observed at a late stage of reaction. A number of phenomena not considered in the model may be: (1) HRP conformational change during reaction affecting the value of rate constants involved; (2) protein oxidation and or heme destruction caused by free radicals attack (Valderrama et al., 2002); (3) increasing of dye extinction coefficient due to dye-phenoxy radical interaction; or (4) phenoxy-radical coupling as the main pathway instead of coupling to AAP due to the increased accumulation. However, HRP catalatic cycle can be ruled out as a competitive pathway to dye formation at this condition (see Fig. 4).

Experimental runs at high peroxide concentration (8.8–300 mM), with hematin as the catalyst showed an increasing initial rate of dye formation with the increase of $H_2O_2$ initial concentration until 50 mM, and decreased afterwards (Fig. 8). End values of dye concentration decreased markedly with the increase of peroxide concentration indicating operative inactivation. In order to test the proposed model at high peroxide conditions, a re-estimation procedure of the model became necessary since a new hematin batch was used for obtaining these data series. Re-estimated constants, selecting optimized values from batch 1 as initial guesses, indicated that hematin batch 2 was slightly more active and less sensitive to peroxide than hematin batch 1 (see Table 2). Fig. 8 illustrates the comparison between experimental and estimated reaction courses (continuous line). The original model was unable to simulate the above mentioned tendency to lower dye-end values and fitting was rather poor i.e. high sum of weighted residuals.

Inactivation routes were proposed for iron porphyrins, either from attack of $H_2O_2$ to resting state and to analogue Compound II, or by inter and intra molecular degradation from the oxoperferryl-π-cation radical (Cunningham et al., 2001). Possible attack of peroxide radicals to the porphyrin were also postulated (Stephenson and Bell, 2005). Our UV/visible inspection of hematin showed an increased bleaching of the Soret band with peroxide concentration, thus suggesting some kind of inactivation (Córdoba et al., 2012b). Moreover, the plateau regions in Fig. 8 were reached faster at higher peroxide concentrations. Thus, inactivation may involve direct $H_2O_2$ interaction with hematin intermediaries rather than of reaction products, e.g., inorganic radicals. On the other hand, reduction of Compound I may become feasible by $H_2O_2$ attack in competition with phenol at these conditions. Therefore, the following routes were incorporated to the original model: (1) reduction of Compound I to Compound II upon $H_2O_2$ attack (i.e., involving $k_{2b}$ constant) and; (2) $H_2O_2$ mediated porphyrin bleaching from Compound II (i.e., involving $k_{bl}$ constant) (see Scheme 1). Fitting results varied significantly with the initial guesses for $k_{bl}$ and the best results were obtained with 0.1 $mM^{-1}\,s^{-1}$. Results of this estimation are shown in Table 2 and Fig. 8. Initial rates and dye end-values of simulated

**Table 2**
Initial guesses and optimized rate constant values of modified models according to Schema 1.

| [$mM^{-1}\ s^{-1}$] | Initial guess value | | Optimized value | | |
|---|---|---|---|---|---|
| | HRP | Hematin | HRP | Hematin | |
| | | | | Original model | Modified model |
| $k_1$ | – | $1.14 \times 10^{-2}$ | [a] | $1.32 \times 10^{-2} \pm 3.0 \times 10^{-4}$ | $1.20 \times 10^{-2} \pm 3.1 \times 10^{-4}$ |
| $k_3$ | – | $7.58 \times 10^{-2}$ | [a] | $13.7 \times 10^{-2} \pm 2.2 \times 10^{-2}$ | $15.1 \times 10^{-2} \pm 2.5 \times 10^{-2}$ |
| $k_{app}$ | $7.5 \times 10^{-3}$ | $3.05 \times 10^{-3}$ | $4.6 \times 10^{-2} \pm 2.7 \times 10^{-3}$ | $2.50 \times 10^{-3} \pm 4.5 \times 10^{-4}$ | $1 \times 10^{-8}$ [b] |
| $k_a$ [$s^{-1}$] | $1.5 \times 10^{-2}$ | $2.24 \times 10^{-3}$ | $1.1 \times 10^{-1} \pm 7.5 \times 10^{-3}$ | $3.91 \times 10^{-3} \pm 2.1 \times 10^{-4}$ | $4.20 \times 10^{-3} \pm 8.4 \times 10^{1}$ |
| $k_i$ | $2.5 \times 10^{-3}$ | – | $5.4 \times 10^{-20}$ [b] | – | – |
| $k_{ii}$ | $2.0 \times 10^{-4}$ | – | $5.1 \times 10^{-4} \pm 1.3 \times 10^{-5}$ | – | – |
| $k_{2b}$ | – | $3.0 \times 10^{-2}$ | [a] | – | $6 \times 10^{-7*}$ |
| $k_{bl}$ | – | $1.0 \times 10^{-1}$ | [a] | – | $1.56 \times 10^{-3} \pm 3.0 \times 10^{-4}$ |
| Initial guess $\sigma^2$ | | | $0.11^2$ [Dye]$^2$ | $0.010^2$ [Dye]$^{0.5*2}$ | $0.010^2$ [Dye]$^{0.5*2}$ |
| Optimized $\sigma^2$ | | | $0.14^2$ [Dye]$^2$ | $0.021^2$ [Dye]$^{0.18*2}$ | $0.020^2$ [Dye]$^{0.005*2}$ |
| Weighted residuals | | | 3919.5 | 4319.5 | 1610.9 |
| $\chi^2$ (95%) | | | 4065.8 | 4360 | 4360 |

[a] Rate constants were fixed according to the optimized values in the table.
[b] Values lying at their lower bound setting after estimation procedure.

profiles approached closer to experimental findings compared to unmodified model, indicating that some of the incorporated routes may be involved. Moreover, weighted residuals were markedly reduced upon estimation of the modified model. In light of the optimized rate constants values, bleaching of hematin appeared as the most relevant side pathway at high peroxide conditions, and showed an optimized value closer to the value encountered by Cunningham for $F_{20}$TPPFeCl(Cunningham et al., 2001). This result was completely in line with simulation results of modified model showing the effect of the added routes: $k_{2b}$ route reduces initial rates of dye formation whereas the $k_{bl}$ route lowers the dye end-value. Thus, reduction of Compound I to Compound II with generation of $HOO^{\bullet}$ appeared to be minor and this was in accordance with the inhibition of oxygen evolvement observed when AAP was present (Fig. 4). On the other hand, $k_{app}$ optimized value was highly reduced upon addition of the new routes. This result indicated that hematin was rather irreversibly inactivated, with the recuperation to resting state almost absent.

Modified model for hematin was less accurate at high peroxide concentrations showing underestimation at $H_2O_2 \geq 50$ mM. It seems that a compensatory reaction with $H_2O_2$ in terms of regeneration of the ferric hematin was not being considered adequately at high $H_2O_2$ concentration in the mechanism. Perhaps the coordination of two $H_2O_2$ molecules and the generation of water with a faster intermediate $E_I$ generation should be included in the mechanism:

$$\text{Por Fe(III)} + 2H_2O_2 \rightarrow \text{Fe(OH)}_2 + H_2O$$

$$\text{Fe(OH)}_2 \rightarrow \text{Por}^{\bullet +}\ \text{Fe(IV)=O} + H_2O$$

Dye end-values were overestimated at $H_2O_2 < 50$ mM. At long reaction times, the dye may even coordinate to Fe in such a way that it may compete with the $H_2O_2$ coordination, especially due to the steric hindrance. This secondary reaction, or coordination of the dye at high concentration of the dye, may also be a reason of the lack of fitting at long reaction times:

$$\text{Fe(Hematin)} + \text{Dye} \rightarrow \text{Fe(Hematin)} - \text{Dye}$$

This complex may be strong and stable or even irreversible due to covalent bonding with the dye. Some parallel pathways may also be involved, e.g., possible iron release upon hematin bleaching or heme destruction by radicals attack (Valderrama et al., 2002).

## 5. Conclusions

We evaluated the action of hematin in comparison to horseradish peroxidase by means of the parametrization of a kinetic model for the co-oxidation of phenol and 4-Aminoantipyrine. The lack of oxygen evolution during reaction provides support to the proposed model as the main route. A sensitivity analysis yielded that four of the ten model rate constants were statistically significant. These four constants were involved in the catalytic steps. Since simulated product formation fit experimental data after parametrization, the involvement of enzyme-identical intermediaries of main catalytic cycle can be postulated for hematin. However, differences were identified not only on the value of the optimized rate constants but also on the pattern of profiles at high $H_2O_2$ concentrations. The values of rate constants encountered for hematin clearly indicated lower activity and lower specificity to phenol over $H_2O_2$ compared to the peroxidase, revealing that the proteic structure around the porphyrin confers higher affinity towards reducing substrates. Moreover, when inactivation routes were incorporated, the parametrization process indicated that hematin bleaches rather than inactivating reversibly via Compound III formation, as originally postulated.

When 4-Aminoantipyrine was absent, oxygen evolved in the hematin system and phenoxy–phenoxy radical coupling could not be detected, in contrast to the enzyme. This was interpreted as formation of peroxyl radicals as has already been established with similar iron porphyrins. Thus, in spite of having similar catalytic intermediaries, the mechanistic action of hematin on peroxide decomposition and oxidations of organic matter may vary involving unspecific radical oxidations as in Fenton chemistry.

The mechanistic findings found in this study may also have a profound impact on the interpretation and optimization of the catalytic performance of hematin towards phenolic substrates in general. Besides, hematin emerges as an attractive HRP-alternative catalyst for the $H_2O_2$ mediated phenol/4-Aminoantipyrine co-oxidation reaction, due to its cost-effective nature and non-polyphenol building ability.

## Acknowledgments

The authors acknowledge the financial support of the National Council of Scientific and Technical Research (CONICET), the National Agency of Scientific and Technological Promotion (ANPCyT-PICT 2010-0788 and PRH-UNC-3), and the National

University of Córdoba (Argentina). Furthermore, the authors acknowledge the collaboration of the Industrial Chemistry Department of the Faculty of Exact, Physical and Natural Sciences of the National University of Córdoba. The authors acknowledge Dr Adriana Brandolín (PLAPIQUI-UNS-CONICET) for her helpful advice and contribution to this manuscript. The authors acknowledge Miss Brittan Hlista (a native english speaker) for the english checking.

## References

Adediran, S.A., Lambeir, A.M., 1989. Kinetics of the reaction of compound II of horseradish peroxidase with hydrogen peroxide to form compound III. Eur. J. Biochem. 186, 571–576.

Akkara, J.A., Wang, J., Yang, D.P., Gonsalves, K.E., 2000. Hematin-catalyzed polymerization of phenol compounds. Macromolecules 33, 2377–2382.

Biava, H., Signorella, S., 2010. Peroxidase activity of dimanganese(III) complexes with the $[Mn_2(\mu\text{-OAc})(\mu\text{-OR})_2]^{3+}$ core. Polyhedron 29, 1001–1006.

Carvalho, R.H., Lemos, F., Lemos, M.A.N.D.A., Vojinovic, V., Fonseca, L.P., Cabral, J.M.S., 2006. Kinetic modelling of phenol co-oxidation using horseradish peroxidase. Bioprocess Biosyst. Eng. 29, 99–108.

Córdoba, A., Magario, I., Ferreira, M.L., 2012a. Evaluation of hematin-catalyzed Orange II degradation as a potential alternative to horseradish peroxidase. Int. Biodeteror. Biodegrad. 73, 60–72.

Córdoba, A., Magario, I., Ferreira, M.L., 2012b. Experimental design and MM2–PM6 molecular modelling of hematin as a peroxidase-like catalyst in Alizarin Red S degradation. J. Mol. Catal. B: Enzym. 355, 44–60.

Cunningham, I.D., Danks, T.N., Hay, J.N., Hamerton, I., Gunathilagan, S., 2001. Evidence for parallel destructive, and competitive epoxidation and dismutation pathways in metalloporphyrin-catalysed alkene oxidation by hydrogen peroxide. Tetrahedron 57, 6847–6853.

De Villiers, K.A., Kaschula, C.H., Egan, T.J., Marques, H.M., 2007. Speciation and structure of ferriprotoporphyrin IX in aqueous solution: spectroscopic and diffusion measurements demonstrate dimerization, but not μ-oxo dimer formation. J. Biol. Inorg. Chem. 12, 101–117.

Dunford, B., 1999. Heme Peroxidases. Wiley-VCH.

Emerson, E., 1943. The Condensation of Aminoantipyrine. II. New Color Test for Phenolic Compounds. Contribution from the Chemical Laboratory of Trinity College.

Fiamegos, Y., Stalikas, C., Pilidis, G., 2002. 4-Aminoantipyrine spectrophotometric method of phenol analysis: study of the reaction products via liquid chromatography with diode-array and mass spectrometric detection. Anal. Chim. Acta 467, 105–114.

Ghosh Datta, S., Dou, X., Shibley, A., Datta, B., 2012. DNA template-assisted modulation of horseradish peroxidase activity. Int. J. Biol. Macromol. 50, 552–557.

Goh, Y.M., Nam, W., 1999. Significant electronic effect of porphyrin ligand on the reactivities of high-valent iron(IV) oxo porphyrin cation radical complexes. Inorg. Chem. 38, 914–920.

Hernández-Ruiz, J., Arnao, M.B., Hiner, A.N.P., García-Cánovas, F., Acosta, M., 2001. Catalase-like activity of horseradish peroxidase: Relationship to enzyme inactivation by $H_2O_2$. Biochem. J. 354, 107–114.

Kalyanararnan, B., Mottleyg, C., Mason, R.P., 1983. A direct electron spin resonance and spin-trapping investigation of peroxyl free radical formation by hematin/hydroperoxide systems. J. Biol. Chem. 258, 3855–3858.

Li, D., Tong, Y., Huang, J., Ding, L., Zhong, Y., Zeng, D., Yan, P., 2011. First observation of tetranitro iron(II) phthalocyanine catalyzed oxidation of phenolic pollutant assisted with 4-aminoantipyrine using dioxygen as oxidant. J. Mol. Catal. A: Chem. 345, 108–116.

Metelitza, D.I., Litvinchuk, A.V., Savenkova, M.I., 1991. Peroxidase-catalyzed co-oxidation of halogen-substituted phenols and 4-aminoantipyrine. J. Mol. Catal. 67, 401–411.

Mifune, M., Sugimoto, K., Iwado, A., Akizawa, H., Motohashi, N., Saito, Y., 2003. Flow injection analysis of hydrogen peroxide using glass-beads modified with manganese(III)-tetra(4-carboxyphenyl)porphine derivative and its analytical application to the determination of serum glucose. Anal. Sci. 19, 569–573.

Mifuni, M., Iwado, A., Akizawa, H., Sugimoto, K., Saito, Y., 2000. Peroxidase-like activity of glass-beads modified with metal-porphines and their analytical applications. Anal. Sci. 16, 1121–1125.

Nagarajan, S., Nagarajan, R., Bruno, F., Samuelson, L.A., Kumar, J., 2009. A stable biomimetic redox catalyst obtained by the enzyme catalyzed amidation of iron porphyrin. Green Chem. 11, 334–338.

Nam, W., Han, H.J., 2000. New insights into the mechanisms of O–O bond cleavage of hydrogen peroxide and *tert*-alkyl hydroperoxides by iron(III) porphyrin complexes. J. Am. Chem. Soc. 122, 8677–8684.

Nicell, J.A., Wright, H., 1997. A model of peroxidase activity with inhibition by hydrogen peroxide. Enzyme Microb. Technol. 21, 302–310.

Odo, J., Sumihiro, M., Okadome, T., Inoguchi, M., Akashi, H., Nakagoe, K., 2009. Peroxidase-like catalytic activity of water-insoluble complex linked Fe(III)-thiacalix[4]arenetetrasulfonate with tetrakis(1-methylpyridinium-4-yl) porphine via ionic interaction. Chem. Pharm. Bull. 57, 1400–1404.

Omuro Lupetti, K., Rocha, F.R.P., Fatibello-Filho, O., 2004. An improved flow system for phenols determination exploiting multicommutation and long pathlength spectrophotometry. Talanta 62, 463–467.

Pirillo, S., Einschlag, F.S.G., Ferreira, M.L., Rueda, E.H., 2010. Eriochrome blue black R and fluorescein degradation by hydrogen peroxide oxidation with horseradish peroxidase and hematin as biocatalysts. J. Mol. Catal. B: Enzym. 66, 63–71.

PSE, 2004. gPROMS Advanced User Guide 1997–2004. Process Systems Enterprise Limited, London.

Rajendiran, N., Santhanalakshmi, J., 2006. Metal tetrasulfophthalocyanines catalysed co-oxidation of phenol with 4-aminoantipyrine using hydrogen peroxide as oxidant in aqueous microheterogeneous system. J. Mol. Catal. A: Chem. 245, 185–191.

Ravichandran, S., Nagarajan, S., Kokil, A., Ponrathnam, T., Bouldin, R.M., Bruno, F.F., Samuelson, L., Kumar, J., Nagarajan, R., 2012. Micellar nanoreactors for hematin catalyzed synthesis of electrically conducting polypyrrole. Langmuir 28, 13380–13386.

Reihmann, M., Ritter, H., 2006. Synthesis of phenol polymers using peroxidases. Adv. Polym. Sci. 194, 1–49.

René, A., Abasq, M., Hauchard, D., Hapiot, P., 2010. How do phenolic compounds react toward superoxide ion? A simple electrochemical method for evaluating antioxidant capacity. Anal. Chem. 82, 8703–8710.

Ribeiro, J.P.N., Segundo, M.A., Reis, S., Lima, J.L.F.C., 2009. Spectrophotometric FIA methods for determination of hydrogen peroxide: Application to evaluation of scavenging capacity. Talanta 79, 1169–1176.

Ryu, J.H., Lee, Y., Do, M.J., Jo, S.D., Kim, J.S., Kim, B.S., Im, G.I., Park, T.G., Lee, H., 2014. Chitosan-*g*-hematin: enzyme-mimicking polymeric catalyst for adhesive hydrogels. Acta Biomater. 10, 224–233.

Sakai, S., Moriyama, K., Taguchi, K., Kawakami, K., 2010. Hematin is an alternative catalyst to horseradish peroxidase for in situ hydrogelation of polymers with phenolic hydroxyl groups in vivo. Biomacromolecules 11, 2179–2183.

Singh, A., Roy, S., Samuelson, L., Bruno, F., Nagarajan, R., Kumar, J., John, V., Kaplan, D.L., 2001. Peroxidase, hematin, and pegylated-hematin catalyzed vinyl polymerizations in water. J. Macromol. Sci. 38A, 1219–1230.

Stephenson, N.A., Bell, A.T., 2005. A study of the mechanism and kinetics of cyclooctene epoxidation catalyzed by iron(III) tetrakispentafluorophenyl porphyrin. J. Am. Chem. Soc. 127, 8635–8643.

Tang, B., Zhang, G.Y., Liu, Y., Han, F., 2002. Studies on catalytic spectrophotometry using β-cyclodextrin polymer–Schiff base metal complex as mimetic enzyme. Anal. Chim. Acta 459, 83–91.

Traylor, T.G., Tsuchiya, S., Byun, Y.S., Kim, C., 1993. High-yield epoxidations with hydrogen peroxide and *tert*-butyl hydroperoxide catalyzed by iron(III) porphyrins: heterolytic cleavage of hydroperoxides. J. Am. Chem. Soc. 115, 2775–2781.

Valderrama, B., Ayala, M., Vazquez-Duhalt, R., 2002. Suicide inactivation of peroxidases and the challenge of engineering more robust enzymes. Chem. Biol. 9, 555–565.

Van Der Zee, J., Barr, D.P., Mason, R.P., 1996. ESR spin trapping investigation of radical formation from the reaction between hematin and *tert*-butyl hydroperoxide. Free Radical Biol. Med. 20, 199–206.

Vlasits, J., Jakopitsch, C., Bernroitner, M., Zamocky, M., Furtmüller, P.G., Obinger, C., 2010. Mechanisms of catalase activity of heme peroxidases. Arch. Biochem. Biophys. 500, 74–81.

Vojinovic, V., Azevedo, A.M., Martins, V.C.B., Cabral, J.M.S., Gibson, T.D., Fonseca, L.P., 2004. Assay of $H_2O_2$ by HRP catalysed co-oxidation of phenol-4-sulphonic acid and 4-aminoantipyrine: characterisation and optimisation. J. Mol. Catal. B: Enzym. 28, 129–135.

Vojinovic, V., Carvalho, R.H., Lemos, F., Cabral, J.M.S., Fonseca, L.P., Ferreira, B.S., 2007. Kinetics of soluble and immobilized horseradish peroxidase-mediated oxidation of phenolic compounds. Biochem. Eng. J. 35, 126–135.